*Math. Model. Nat. Phenom.*
**Vol. 5, No. 1, 2010, pp. 84-105**
DOI: 10.1051/mmnp/20105104

# Mechanisms of Cell Motion in Confined Geometries

**R. J. Hawkins*** **and R. Voituriez**

UMR 7600, Université Pierre et Marie Curie/CNRS, 4 Place Jussieu
75255 Paris Cedex 05 France

**Abstract.** We present a simple mechanism of cell motility in a confined geometry, inspired by recent motility assays in microfabricated channels. This mechanism relies mainly on the coupling of actin polymerisation at the cell membrane to geometric confinement. We first show analytically using a minimal model of polymerising viscoelastic gel confined in a narrow channel that spontaneous motion occurs due to polymerisation alone. Interestingly, this mechanism does not require specific adhesion with the channel walls, and yields velocities potentially larger than the polymerisation velocity of the gel. We then study the effect of the contractile activity of myosin motors, and show that whilst it is not necessary to induce motion, it quantitatively increases the velocity of motion in the polymerisation mechanism we describe. Our model qualitatively accounts for recent experiments which show that cells without specific adhesion proteins are motile only in confined environments while they are unable to move on a flat surface. It also constitutes a first step in the study of cell migration in more complex confined geometries such as living tissues.

**Key words:** cell motility, active gel, theory, hydrodynamics
**AMS subject classification:** 76A10, 76A15, 76D08, 92C05, 92C17

## 1. Introduction

Identifying and testing simple mechanisms of cell motion is an interdisciplinary challenge of interest not only to biology but also to mathematical and physical sciences, with important applications to medical and technological sciences. Many studies have naturally focussed on cells crawling on a glass substrate, however in biological systems cells often move within a more complex envi-

*Corresponding author. E-mail: rhoda.hawkins@physics.org

ronment. There is an obvious need to better understand cell motion within environments such as living tissues. One aspect of such environments is that of geometric confinement. In this article we consider the question of cell motion in confinement building on the model first presented in [12].

Biological systems usually have low Reynolds number, meaning viscous forces dominate over inertial forces. Since inertia is negligible, sustained motion requires a constant input of energy. Systems driven out of equilibrium by an internal or external energy source are termed active. Examples of active systems range from animal flocks [31] and bacterial colonies [7, 11] to vibrated granular media [25]. The cell cytoskeleton is a striking example of such an active system. It is a network of long semi-flexible filaments made up of protein subunits, interacting with other proteins such as motor proteins. The filaments, for example actin, use the chemical energy of ATP hydrolysis to polymerise and the motor proteins use this chemical energy to exert active stresses that deform the network [1, 26].

Two main different mechanisms for cell motility have now been distinguished, namely polymerisation (or treadmilling referring to polymerisation of a filament at one end and depolymerisation at the other end) and contractility due to molecular motors. Motion due to polymerisation [2, 24] and to contractility [26] have now been observed experimentally and studied theoretically [14, 15, 16, 32, 33, 35] and numerically [22, 23]. In all these models the essential ingredients for motion are an energy input to overcome dissipation and sufficient adhesion or friction with a substrate to transfer momentum. The common picture of a cell crawling on a surface is: the thin protrusion at the leading edge of the cell (called the lamellipodium) builds strong adhesion points with the substrate and pushes forward its membrane by polymerising actin. At the back of the cell, the cell body contracts and breaks the adhesion points. The resulting overall cell velocity is then limited by the actin polymerisation rate (which however varies substantially between cell types), in agreement with available experimental data [5, 27, 30].

Recent experiments [18, 21] have observed both in-vivo and in-vitro that mutant cells that are unable to produce active integrin complexes (adhesion proteins) display sustained motility in confined environments (tissues or synthetic polymeric gels), whereas they fail to move on flat two-dimensional substrates. Motion in confinement is also observed even without myosin [18]. These observations suggest the existence of an alternative mechanism of motility to the adhesion dependent picture of a cell crawling on a surface. The ability of these cells to move in confinement but not on a surface suggests that confinement plays a vital role in this mechanism of motion.

In this article we discuss a new, simple mechanism of motility which relies strongly on geometric confinement and which accounts for these observations. Interestingly, it does not require strong specific adhesion, and yields velocities potentially larger than the polymerisation velocity. This confinement induced motility mechanism is driven primarily by actin polymerisation at the cell membrane. We also discuss the role of active contractility due to the action of molecular motors. The model relies on the hydrodynamic theory of active gels [14, 15, 16], which we review. Such a mathematical model of motion in simple confined geometries is motivated by experiments in microfabricated channels [8] and could help in understanding the mechanisms of cell migration is complex crowded environments such as living tissues.

In Section 2. we introduce the simplest form of our model; that of a polymerising viscoelastic gel confined in a long thin channel. After discussing the pressure dependence of the polymerisation

and the friction with the channel walls, we calculate the pressure and velocity profile and discuss the hypotheses we make to model a finite moving biological cell. In Section 3. we review the theory of active gels and discuss the role of the contractile active stress induced by molecular motors in the model presented in Section 2. Finally, in Section 4., we broaden our discussion of confinement in a straight channel by introducing a tilt to the channel wall thereby making an initial step towards more complex confined geometries.

# 2. Polymerising gel model

In this section we introduce our model starting from a polymerising viscoelastic gel confined in a channel. We then refine this model to mimic motile cells in confinement.

## 2.1. A viscoelastic gel in an infinitely long channel

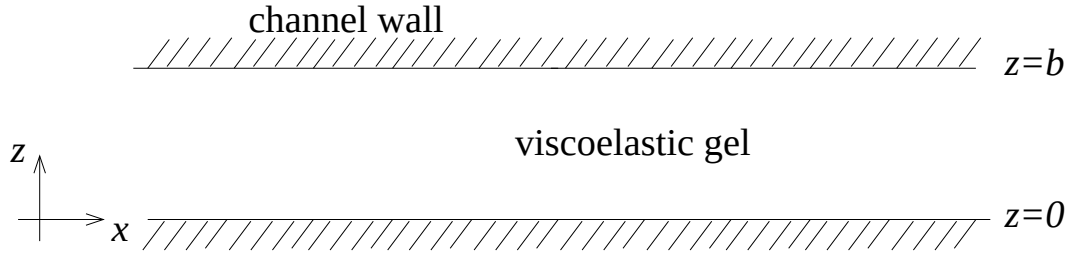


Figure 1: Channel geometry.

Initially we consider a passive incompressible viscoelastic film confined in a bidimensional channel of width $b$ and infinite length as shown in Figure 1. In such a single fluid model, for the polymer plus the solvent, it is reasonable to assume global incompressibility. The experimental observations motivate incompressibility since the cell volume appears to be roughly constant when it changes shape to fit into the channels. The bidimensional geometry mimics the experimental conditions of channels of rectangular cross-section. The case of a cylindrical confining channel can be treated with minor modifications. The axes are defined with $x$ along the channel and $z$ across it. The confining walls are placed at $z = 0$ and $z = b$. We denote the components of the velocity of the gel by $v_i$, the strain rate by $u_{ij} = (\partial_i v_j + \partial_j v_i)/2$, and the vorticity tensor by $\omega_{ij} = (\partial_i v_j - \partial_j v_i)/2$. We assume that the gel is described by a linear Maxwell model of viscoelasticity, which simply represents the material as an elastic spring in series with a purely viscous drag. Therefore the constitutive equation relating the strain rate to the deviatory stress tensor $\sigma_{ij}$ is written as:

$$2\eta u_{ij} = \left(1 + \tau \frac{\mathrm{D}}{\mathrm{D}t}\right) \sigma_{ij}, \tag{2.1}$$

where $\eta$ is the shear viscosity and $\tau$ is the typical relaxation time of the drag related to the elastic modulus $E = \eta/\tau$. To ensure invariance with respect to translation and rotation, we use the co-rotational derivative $\frac{\mathrm{D}\sigma_{ij}}{\mathrm{D}t} = \frac{\partial\sigma_{ij}}{\partial t} + v_k\partial_k\sigma_{ij} + \omega_{ik}\sigma_{kj} + \omega_{jk}\sigma_{ki}$ [19], instead of the usual time derivative. For very short relaxation times $\tau$, equation (2.1) describes a viscous fluid and for long relaxation times it describes an elastic material. For polymer gels in practice $\tau$ widely varies with parameters such as polymer concentration, pressure, or the cross-linker concentration. For dilute polymer gels, $\tau$ is very small and the gel behaves as a viscous fluid. At higher concentrations, or for more cross-linked gels, $\tau$ becomes very large and the gel behaves as an elastic medium. In what follows we assume that the gel is in either of the two regimes. We assume that our gel is incompressible such that, in the case of no polymerisation or depolymerisation,

$$\nabla \cdot \mathbf{v} = \partial_x v_x + \partial_z v_z = 0, \tag{2.2}$$

which means that $\tau$ depends on pressure $P$ only. We define a critical pressure such that $\tau(P < P^*) = 0$ (viscous regime) and $\tau(P > P^*) = \infty$ (elastic regime). Initially we consider the gel to be in the viscous fluid regime ($\tau = 0$). In the limit of low Reynolds number viscous forces dominate over inertial forces and the Navier-Stokes equation simplifies to the balance of forces;

$$\partial_i(\sigma_{ij} - P\delta_{ij}) = 0. \tag{2.3}$$

Finally as in [14] we assume viscous friction at the channel walls $z = 0$ and $z = b$, and write $\sigma_{xz} = \xi v_x$ where $\xi(x)$, which can potentially be a function of $x$, characterises the friction and will be described in more detail below.

## 2.2. A viscoelastic gel in a thin, infinitely long channel

We now derive the dynamical equations of the system in the lubrication approximation ( $b \ll L$ where $L$ is the typical length of the system). In this limit the variation of velocity field $v_i(x, z)$ along the channel (in the $x$ direction) can be taken as negligible as compared to variations along $z$. The force balance (equation (2.3)) therefore becomes;

$$\begin{aligned} \partial_z P &= 0 \\ \partial_x P &= \eta\partial_z^2 v_x. \end{aligned}$$

In this approximation therefore $\partial_x P = \frac{\mathrm{d}P}{\mathrm{d}x}$. With the symmetry $v_x(x, 0) = v_x(x, b)$ and the viscous friction $\sigma_{zx}(z = 0) = \xi v_x(x, 0)$ this leads to

$$v_x(x, z) = -\frac{1}{2\eta}\frac{\mathrm{d}P}{\mathrm{d}x}\left((b - z)z + \frac{b\eta}{\xi}\right) \tag{2.4}$$

and with the incompressibility condition equation (2.2)

$$v_z(x, z) = \frac{1}{12\eta}\frac{\mathrm{d}^2P}{\mathrm{d}x^2}\left((3b - 2z)z + \frac{6b\eta}{\xi}\right)z - \frac{\mathrm{d}P}{\mathrm{d}x}\frac{\mathrm{d}\xi}{\mathrm{d}x}\frac{bz}{2\xi^2} + v_z(x, 0). \tag{2.5}$$

Defining the average velocity along the channel $v(x) = (1/b)\int_0^b v_x(x,z)dz$, we obtain the following proportional relationship between the fluid flux and the pressure gradient;

$$v(x) = -\frac{b^2}{12\eta}\left(1 + \frac{6\eta}{b}\xi^{-1}\right)\frac{\mathrm{d}P}{\mathrm{d}x}, \tag{2.6}$$

which is therefore of the form of Darcy's law.

## 2.3. Self-polymerisation

To this passive viscoelastic gel, we add active properties to describe a biological active gel. The first active property we consider is the out-of-equilibrium polymerisation of the gel. Actin monomers are added to actin filaments in a cell by the consumption of the biological fuel ATP. Other proteins regulate the nucleation and polymerisation of actin filaments. It is commonly observed that actin polymerisation activators such as WASP proteins preferentially locate along the cell membrane [1, 5]. In the case of dendritic cells, actin filaments appear to anchor perpendicularly to the cell membrane, forming structures called podosomes where polymerisation takes place [4]. For these reasons we suppose that the gel is polymerised at the gel/wall interface with speed $v_p$, therefore inducing an inward flow of actin, $v_z(x, z = 0) = -v_z(x, z = b) = v_p$ (see Figure 2). The

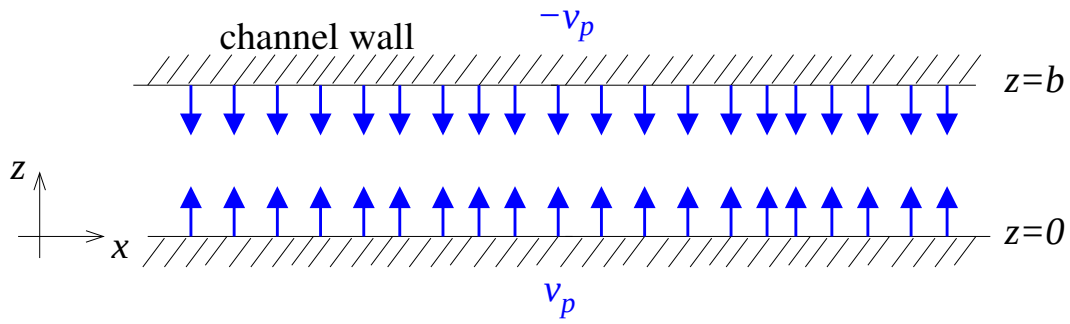


Figure 2: Polymerising gel in a channel. Blue arrows show the inward flow due to polymerisation normal to the channel walls.

model as so far described is therefore equivalent to a viscous fluid in an infinitely long thin channel into which fluid is injected perpendicularly from the walls. The polymerisation is balanced by depolymerisation to conserve mass. When calculating the velocity profile, equations (2.4) and (2.5), as we do to obtain Figures 6, 8-12, the depolymerisation rate $k_d$ should also be included in the incompressibility condition (2.2) and therefore appears in equation (2.5) in the additional term $-k_d z$. Here however we focus on the average velocity along the channel $v$ and write;

$$\frac{\mathrm{d}}{\mathrm{d}x}(bv) = 2v_p - k_d b. \tag{2.7}$$

Equation (2.6) then becomes;

$$\frac{\mathrm{d}}{\mathrm{d}x}\left[b^3(1+\tilde{\xi}^{-1})\frac{\mathrm{d}P}{\mathrm{d}x}\right] = -12\eta(2v_p - bk_d), \tag{2.8}$$

where $v_p$ and the nondimensional friction $\tilde{\xi} \equiv \xi b/6\eta$ can be a priori functions of $P$ and $x$.

## 2.4. Boundary conditions

Two boundary conditions are needed to determine the pressure profile $P(x)$ from equation (2.8). We neglect the friction with the surrounding fluid in the channel and set the pressure at the leading edge, which is assumed to coincide with the point $x = L$, as $P(L) = 0$, which gives the first boundary condition. Note that if the pressure at the leading edge is finite due to an external force, our results apply with an unimportant shift in the pressure field. We look for stationary states with broken symmetry and positive velocity and therefore the pressure is a decreasing function of $x$. If the system is large enough, we assume that at the front the gel is in the fluid phase but that at a certain point the increasing pressure towards the back will reach the threshold $P^*$ above which the gel is in the elastic regime. We therefore consider the gel in the channel as consisting of a fluid part at the front, travelling at velocity $V$ and an elastic part at the back with velocity zero, extending to $x = -\infty$ (see Figure 3). The boundary between the two phases, which we label as $x = 0$, must

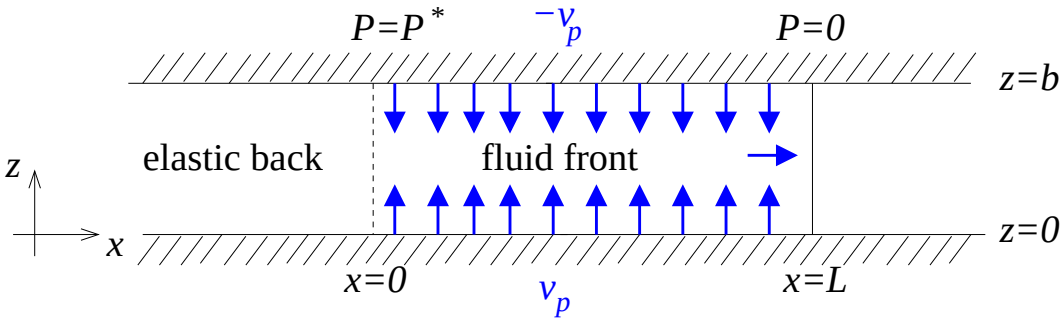


Figure 3: Diagram of the model showing channel geometry and viscous and elastic regimes. Blue arrows show the flow direction

move at the same velocity as the fluid front $V$ for a constant length $L$ of the fluid part ($L$ is constant for incompressible flow). The fact that the velocity of the elastic region should be zero gives the second boundary condition needed to calculate the pressure field: $v(0) = 0 = \frac{\mathrm{d}P}{\mathrm{d}x}|_{x=0}$. The self-consistent condition $P(0) = P^*$ gives in turn an equation enabling the calculation of the length $L$ of the fluid front. We then write that the velocity $V$ of the front is given by the calculated velocity of the flow plus the polymerisation velocity at the leading edge $v(L) + v_p(L)$. We stress that the flow velocity is *forward*, i.e. in the same direction as the moving leading edge. Such a forward flow relies on the existence of an elastic region at the back. Such a denser elastic region at the back, called the uropod, is indeed well reported in dendritic cells [28], and is characterised by a higher concentration of cross-linkers. Such an increased concentration of cross linkers would increase the relaxation time $\tau$ (and therefore elastic nature) further beyond that caused by the pressure gradient of the homogeneous incompressible case described here. It is worth noting that the pressure we are discussing here is the mechanical pressure exerted by the fluid due to the force generated by the polymerisation against the confining walls. Real cells are also affected by osmotic pressure due

to differing concentrations of molecules across the cell membrane. We do not discuss potential contributions from osmotic pressure here.

## 2.5. Pressure dependent friction

Qualitatively, the value of the length $L$ is dictated by the steepness of the pressure gradient, and therefore by the friction $\tilde{\xi}$. If $\tilde{\xi}$ is small, then only very long fluid fronts can move. However in this section we show quantitatively that the coupling of $\tilde{\xi}$ with the pressure field actually enables short fluid fronts to move even with a low bare friction (such as that mimicking integrin knock-out experiments by [18]).

Following [9] we argue that the friction coefficient $\tilde{\xi}$ for a polymeric gel depends on the normal constraint. Qualitatively a high normal constraint increases the attachment rate of polymers onto the channel walls by lowering the entropic barrier, and decreases the detachment rate.

In a gel moving at $v_0$, a single filament attached to the surface for a typical time $\tau_a$ will experience a force $F = Ev_0\tau_a$ where $E$ is an elastic modulus. If there are $n$ filaments and the probability of a filament being attached is $P_a$ the total frictional force will be given by $F_{\text{fric}} = nP_aEv_0\tau_a$. The attachment probability $P_a$ will be given by the Fokker-Planck equation

$$\frac{\mathrm{d}P_a}{\mathrm{d}t} = \frac{1 - P_a}{\tau_d} - \frac{P_a}{\tau_a}$$

where $\tau_d$ is the typical time a filament stays detached. If the number of connected filaments changes slowly enough we can take the steady-state solution $P_a = \frac{\tau_a}{\tau_a+\tau_d}$ and therefore

$$F_{\text{fric}} = \frac{nEv_0\tau_a^2}{\tau_a + \tau_d}.$$

We make the assumption that $\tau_a \gg \tau_d$ which corresponds to the case where the filaments are mostly attached and the friction is then dominated by the detachment rate $F_{\text{fric}} \approx nEv_0\tau_a$. If the speed of the gel at the surface is relatively small, mechanical breakage of filaments can be neglected and the detachment rate of filaments $1/\tau_a$ is given by the chemical off rate which is proportional to $\exp(-W/k_BT)$ where $W$ is the energy barrier for dissociation which is proportional to the normal constraint $W \propto (P - \sigma_{nn})$ and $k_B$ is the Boltzmann constant and $T$ the temperature. This then leads to $F_{\text{fric}}/v_0 \propto e^{\beta(P-\sigma_{nn})}$ where $\beta$ is a positive constant of dimensions of inverse pressure that characterises the pressure dependence of the friction. Therefore the friction coefficient is written as

$$\tilde{\xi} = \tilde{\xi}_0 e^{\beta(P-\sigma_{nn})}, \tag{2.9}$$

where in our geometry of straight channel walls the normal stress $\sigma_{nn} = \sigma_{zz}$ for both walls at $z = 0$ and $z = b$.

## 2.6. Pressure dependent polymerisation

We use a standard ratchet model for the polymerisation of a filament against a barrier following [6]. In the simplest ratchet model the polymerisation speed of a filament at the cell membrane is

given by the bare attachment rate $k_{\rm on}$ in the absence of any force multiplied by the probability of thermal fluctuations producing a gap large enough for a new subunit to attach (see Figure 4). The

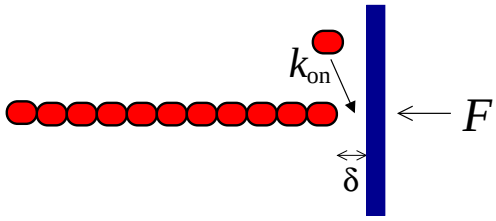


Figure 4: Cartoon of a ratchet model of filament polymerisation.

energy required for a gap the size of a subunit $\delta$ is given by $F\delta$, where $F$ is the load which in our case is proportional to the normal constraint $(P - \sigma_{nn})$. Therefore the polymerisation speed is given by $v_p = k_{\rm on}\delta e^{-F\delta/k_BT}$ which we write as

$$v_p = v_p^0 e^{-\alpha(P-\sigma_{nn})} \tag{2.10}$$

where $v_p^0 = k_{\rm on}\delta$ and $\alpha$ is a positive constant. In this minimal model outlined here we are assuming the filament consists of a single protofilament (in actuality actin has two) and we neglect the dissassociation rate $k_{\rm off}$ from the polymerising end (known as the barbed or plus end). In other words we are assuming that all the depolymerisation occurs at the minus end of the actin filament. Implicit in the model outlined here is also the assumption that the diffusion over the distance $\delta$ is fast compared to the rate of addition of subunits $k_{\rm on}$ and therefore does not influence the polymerisation speed.

## 2.7. Calculation of the pressure profile

Equations (2.9) and (2.10) make equation (2.8) an autonomous equation for $P$, which is completed by the two boundary conditions discussed above in Section 2.4. To our knowledge, such an equation cannot be solved analytically in the general case. However in the regime of small $\alpha$ (defined by $\alpha P^* \ll 1$), $v_p$ can be taken as constant and an analytical approximation scheme can be proposed, which enables a discussion of the motility mechanism.

We first neglect the stress due to the velocity, $\sigma_{nn}$, in equation (2.9) and write the friction coefficient as $\tilde{\xi} \approx \tilde{\xi}_0 e^{\beta P}$. This assumption underestimates the friction, and therefore the pressure field. With these approximations equation (2.8) can be integrated twice analytically and yields an implicit equation for the pressure field to lowest order $P^0$:

$$P^0 + \frac{\tilde{\xi}_0^{-1}}{\beta}(1 - e^{-\beta P^0}) = \frac{6\eta(2v_p^0 - bk_d)}{b^3}(L^2 - x^2). \tag{2.11}$$

where we have implemented the boundary conditions, $P(L) = 0$ and $\frac{\mathrm{d}P}{\mathrm{d}x}|_{x=0} = 0$, as discussed in Section 2.4. This first expression $P^0$ gives a lower bound of the pressure field, and provides a satisfactory approximate as shown by the dotted blue curve in Figure 5.

To improve on this estimate, we use $P^0(x)$ to determine the lowest order velocity profile $v_i^0(z)$ and calculate $\sigma_{zz}^0 = 2\eta\partial_z v_z^0$. The velocity profile is calculated using equations (2.4) and (2.2) with the calculated pressure. Equation (2.8) is then resolved using this calculated value of $\sigma_{zz}^0$ for $\sigma_{nn}$, yielding the next order $P^1(x)$ which in turn can be used for further iterations. This result is the dot-dashed green line plotted in Figure 5. Using realistic values for the parameters corresponding to the actin cytoskeleton, used in [9] and [3], the iteration procedure converges rapidly.

In the general case of finite $\alpha$, the first iteration giving $P^0(x)$ has to be performed numerically, and then the same procedure applies. As shown by the dashed red line in Figure 5 including the pressure dependence of the polymerisation speed ($\alpha > 0$) decreases the pressure compared to $\alpha = 0$. This is expected since the pressure is built up by the polymerisation itself.

To show the impact of the pressure dependence of the friction the result for $\beta = 0$ is also shown in Figure 5 by the black line. Clearly this coupling greatly enhances the pressure.

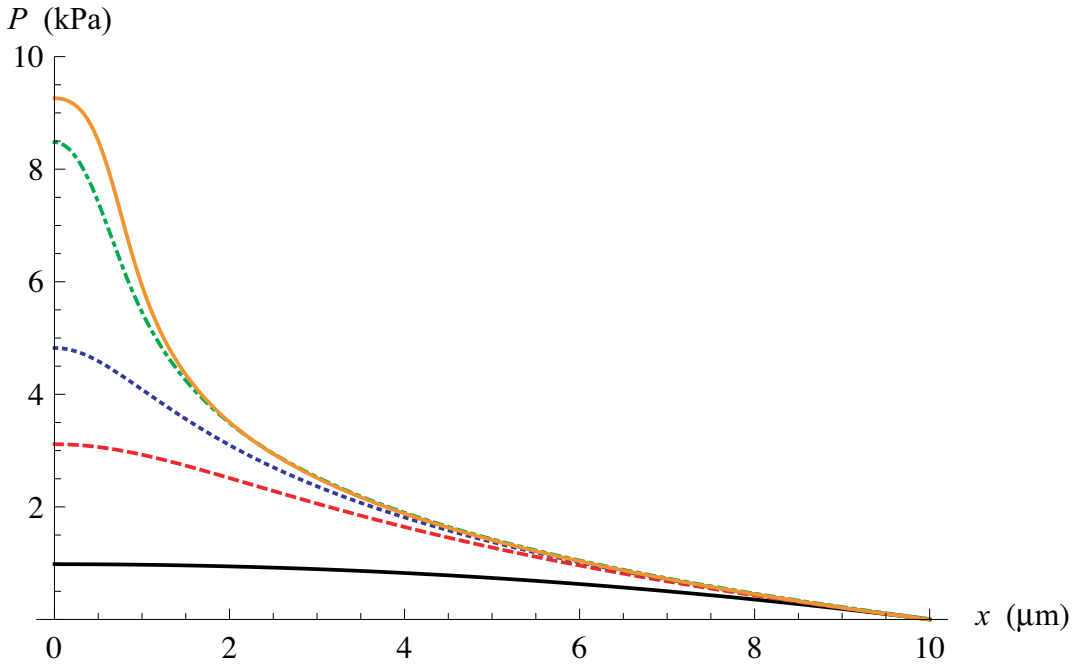


Figure 5: Pressure profile. In order of increasing pressure the curves are: solid black: numerical value $P^0$ for $\beta = 0$, $\alpha = 0.01\text{kPa}^{-1}$; dashed red: numerical value $P^0$ for $\beta = 1\text{kPa}^{-1}$ and $\alpha = 0.01\text{kPa}^{-1}$; dotted blue: analytical expression equation (2.11) for $\beta = 1\text{kPa}^{-1}$, $\alpha = 0$; dot-dashed green: numerical value $P^1$ for $\beta = 1\text{kPa}^{-1}$, $\alpha = 0$; solid orange: numerical value $P^1$ for $\beta = 1\text{kPa}^{-1}$, $\alpha = 0$ for an active polymerising gel (see Section 3.4.). Other parameters (estimates from [3, 9]): $L = 10\mu$m, $b = 1\mu$m, $\eta = 10$kPa s, $k_d = 0.1s^{-1}$, $v_p^0 = 0.1\mu\text{m}s^{-1}$, $\xi_0 = 0.1$kPa s $\mu\text{m}^{-1}$. $v_p^0$ is taken as the speed of dendritic cells on a surface which is expected to be the actin polymerisation speed [30]. $\xi_0$ is taken as very small (lowest estimate in [9] which is 100 fold smaller than in keratocytes [14, 15, 16]) to mimic the low adhesion of integrin knockout dendritic cells.

## 2.8. Velocity profile

Substituting the pressure as calculated in Section 2.7., into equations (2.4) and (2.5) allows us to calculate the velocity profile plotted as blue arrows (filled arrow heads) in Figure 6. For simplicity we use the first iteration, $P^0(x)$. We use $\alpha = 0.01$, $\beta = 1$ and other parameters as in Figure 5.

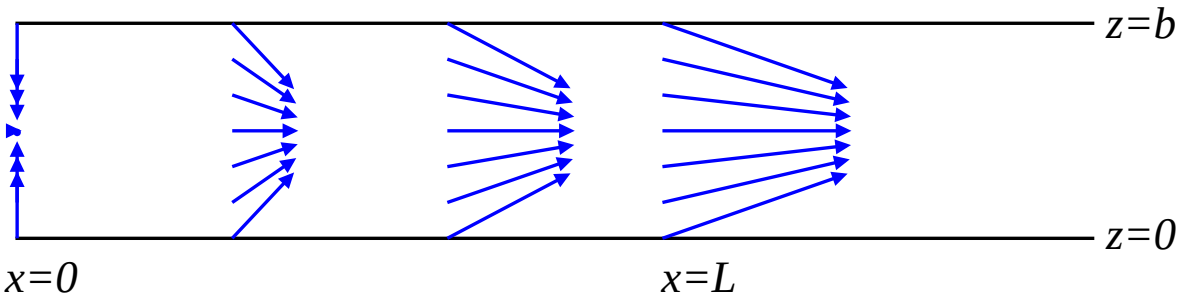


Figure 6: Velocity profile (equations (2.4) and (2.5)) (blue, filled arrow heads) for a polymerising gel in a thin channel.

## 2.9. Modelling a finite cell

We now consider the extra hypotheses required to more realistically model a moving biological cell. Initially we considered an infinitely long system which as from Section 2.4. we consider to be made up of a fluid front $x > 0$ and an elastic back $x < 0$. Also in Section 2.4. we introduced the leading edge located at $x = L$. Instead of an open system extending to $x = -\infty$ we now assume that the elastic regime is a finite region mimicking the uropod observed at the back of the cell [28]. Additionally, we assume $\beta P^* \gg 1$ such that the friction of the uropod with the channel walls is very large, enforcing $v(0) = 0$. To conserve the total cell mass, we further assume that in the uropod the gel depolymerises at the speed of the leading edge $V = v(L) + v_p(L)$ (which defines the over all speed of the cell). A high depolymerisation rate in the uropod can be justified by the high pressure and a depletion of free actin monomers due to the forward flow. This high depolymerisation rate refers to the depolymerisation in the elastic regime and does not refer to the depolymerisation in the fluid region which we assume, as stated previously, is constant. With these hypotheses, the model presented above mimics a cell moving in a channel with velocity $V$, and shows that the confinement induced motility mechanism can indeed be used by cells. Interestingly, for the parameter values used in Figure 5 the front velocity is calculated to be $\sim 10\mu$m/min which

is close to the velocity that can be reached by dendritic cells in collagen matrices [18] and in channels (up to $12 - 15\mu$m/min) [8] which significantly is larger than the polymerisation velocity taken as the speed on a flat surface, $4 - 6\mu$m/min [13].

## 2.10. Motility in confinement versus on a surface

The mechanism we have described produces a forward flow which relies on a pressure build up to $P^*$ in the gel, here induced by confinement. In order to reach a high enough pressure the system needs to be long enough. An estimation of the minimal system size $L$ is given by taking $x = 0$ and $P = P^*$ in equation (2.11):

$$L^2 = \frac{b^3}{6\eta(2v_p^0 - bk_d)} \left( P^* + \frac{\tilde{\xi}_0^{-1}}{\beta}(1 - e^{-\beta P^*}) \right) \tag{2.12}$$

If the friction $\xi$ is small the minimal system size is large. However, due to the exponential dependence of the friction on the pressure, the effective friction can reach large values even with a small bare friction coefficient $\xi_0$. Therefore, by increasing the pressure in the confined channel the polymerising gel is able to build up enough friction to move forwards for a finite $L$.

Equation (2.12) shows that $L$ increases faster than linearly with $b$, indicating that if the channel is too wide the mechanism we describe would not be sufficient to produce forward motion for a finite system size. In the case of a gel on a flat open substrate the typical confining length $b$ is large (of the order of the cell size) and therefore the length $L$ necessary to build a strong pressure gradient is large ($L >$ cell size). Significantly, if the pressure remains below $P^*$, no elastic phase is formed, thus preventing forward flow. In this case our model therefore suggests a retrograde flow, that is in the opposite direction to the moving leading edge. Intuitively if there is no elastic back to push off from, the flow of actin will be backwards due to the flow induced by the polymerisation at the leading edge. Such a retrograde flow of actin has been previously modelled and observed for lamellipodia [14, 15, 16, 34] on flat substrates. The motility mechanism for lamellipodia relies on protrusion of the leading edge by actin polymerisation and adhesion to the substrate followed by contraction and detachment of the rear of the cell.

It is also interesting to note that since the pressure gradient in a cell on a surface is much weaker than in the confined case, the friction with the substrate remains close to its bare value, $\xi_0$, yielding a much smaller momentum transfer with the substrate. Since the friction remains close to its bare value $\xi_0$, we expect the cell motility on a surface to be more sensitive to alterations of the bare friction coefficient that for the case in confinement, as has been observed experimentally for cells without functional adhesion molecules [18, 21].

The flow direction, and therefore the direction of the pressure gradient in the gel, constitutes the main difference between the confinement induced mechanism of motility that we discuss here and the standard picture of cells lying on flat substrates.

Experimentally the pressure field can be quantified indirectly by measuring the effective contact area of the cell membrane using Reflection Interference Contrast Microscopy (RICM). Figure 7 shows clearly that for a dendritic cell confined in a channel a larger contact area at the back of the

cell is seen, indicating a backward pressure gradient in qualitative agreement with our theoretical prediction.

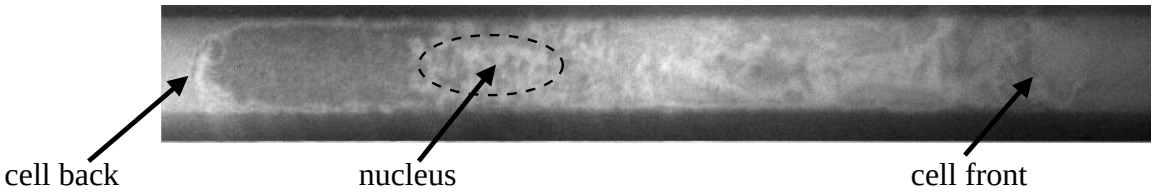


Figure 7: RICM image [12] of a dendritic cell moving (to the right) in a channel of $4\mu$m width. The dark zone at the back of the cell (left) indicates a large contact of the membrane with the channel wall (independent of the nucleus, dotted line), and therefore a high normal constraint, compared to the front (right).

# 3. Active gel model

So far the only "active" (out-of-equilibrium) property we have considered is the self-polymerisation. In this section we introduce the active stress produced in our case by the activity of molecular motors such as myosin. The extension of the hydrodynamic equations for a passive gel, discussed in Section 2.1., to include such an active stress is known as the theory of active gels. It has been developed over recent years [14, 15, 16, 20, 29] and is proving to be successful in describing a wide variety of biological phenomena. Here we provide an outline of the main equations.

## 3.1. Polar gel

Before we consider the active terms we first extend the equations for a viscoelastic gel given in Section 2.1. to the case of a polar viscoelastic gel. We assume the directions of the actin filaments are described by the normalised polarisation field $\mathbf{p} = (\cos\theta, \sin\theta)$ where $\theta$ is the angle with the $x$ axis. Including polarisation the constitutive equation (2.1) in the viscous fluid limit ($\tau \to 0$) becomes;

$$2\eta u_{ij} = \sigma_{ij} - \frac{\nu}{2}(p_i h_j + p_j h_i) + \frac{1}{2}(p_i h_j - p_j h_i), \tag{3.1}$$

where

$$h_i = -\frac{\delta F}{\delta p_i} + \lambda' p_i$$

is the field conjugate to the polarisation, called the molecular field, where $F$ is the free energy. The molecular field is only defined within the transformation $\mathbf{h} \to \mathbf{h} + \lambda'\mathbf{p}$, where $\lambda'$ is an arbitary

function of time and space, since this transformation leaves the torque $\mathbf{\Gamma} = \mathbf{p} \times \mathbf{h}$ unchanged. The standard free energy for a polar liquid crystal is given by the Frank elastic energy [10]

$$F = \int \mathrm{d}x\mathrm{d}z \left[ \frac{K_1}{2}(\nabla \cdot \mathbf{p})^2 + \frac{K_3}{2}(\nabla \times \mathbf{p})^2 \right] \tag{3.2}$$

where $K_{1,3}$ are the splay and bend elastic moduli. In two dimensions the twist term is zero. In the one constant approximation $K_1 = K_3 = K$ this leads to

$$h_i = K\nabla^2 p_i + \lambda' p_i.$$

The molecular field is conveniently written in terms of its components parallel and perpendicular to the polarisation;

$$\begin{aligned} h_{\parallel} =& h_x p_x + h_z p_z = -K((\partial_x\theta)^2 + (\partial_z\theta)^2) + \lambda' \\ h_{\perp} =& h_x p_z - h_z p_x = K\nabla^2\theta. \end{aligned}$$

The second term of the right hand side of equation (3.1) is the coupling between the mechanical stress and the polarisation field, characterised by the coefficient $\nu$ as is standard for liquid crystal hydrodynamics. The third term of the right hand side of equation (3.1) is the antisymmetric part of the stress tensor describing the torque acting on each volume element.

The equation for the polarisation flux is given by

$$\frac{\mathrm{D}p_i}{\mathrm{D}t} = \frac{1}{\gamma}h_i - \nu u_{ij} p_j \tag{3.3}$$

where $\gamma$ is the rotational viscosity. The derivative is the co-rotational derivative $\frac{\mathrm{D}\phi_i}{\mathrm{D}t} = \frac{\partial\phi_i}{\partial t} + (v_k\partial_k)\phi_i + \omega_{ij}\phi_j$ to ensure invariance with respect to rotation as well as translational flow.

In our model we assume normal outwards anchoring at the walls, consistent with available experimental observations. As assumed for models of the lamellipodium [17] we assume normal anchoring at the front. This imposes the symmetry breaking such that the polarisation points forwards (see black arrows in Figures 8 and 9). The polarisation in our case is therefore imposed as $\theta = -\frac{\pi}{2}(1 - \frac{2z}{b})$.

## 3.2. The active contribution

We are finally ready to add the active contribution to the polar gel. The active stress is given by $\sigma_{ij}^{\mathrm{active}} = \tilde{\zeta}\Delta\mu\, p_i p_j$ ([14, 15, 16]) where $\Delta\mu$ is the chemical potential of ATP hydrolysis which provides the energy to the molecular motors driving the system out of equilibrium. The coefficient $\tilde{\zeta}$ determines the nature and strength of the activity and it is to linear order proportional to the myosin concentration. In general the myosin concentration and therefore $\tilde{\zeta}$ may not be homogeneous and we therefore allow it to vary with $x$. Acto-myosin systems are thought to be contractile which corresponds to $\tilde{\zeta} < 0$. With this active stress the constitutive equation (3.1) becomes;

$$2\eta u_{ij} = \sigma_{ij} - \frac{\nu}{2}(p_i h_j + p_j h_i) + \frac{1}{2}(p_i h_j - p_j h_i) + \tilde{\zeta}\Delta\mu\, p_i p_j. \tag{3.4}$$

In general the equation for the polarisation flux (3.3) also gains an extra term due to the activity. This term, $\lambda\Delta\mu\, p_i$, is characterised by the coefficient $\lambda$, which if positive tends to align the filaments enhancing the local polarisation. However if the polarisation has a fixed modulus, as in the case we consider here, this term simply modifies the parallel component of the molecular field $h_\parallel$ (modifying $\lambda'$) which is itself determined by the modulus of the polarisation. Using this modified molecular field $\tilde{h_i} = h_i + \gamma\lambda p_i$ in equation (3.4) simply changes the coefficient $\zeta$ to $\tilde{\zeta} = \zeta + \lambda\nu\gamma$. For simplicity we therefore directly wrote $\tilde{\zeta}$ in equation (3.4) and leave the polarisation flux as in equation (3.3).

## 3.3. The thin channel approximation

It is also useful to consider the lubrication approximation for a thin channel $b \to 0$. The force balance equation (2.3) in this case leads to

$$\partial_x P = \eta\partial_z^2 v_x - \tilde{\zeta}\Delta\mu\,\partial_z(\sin 2\theta)$$

with the appropriate parallel component of the molecular field $\tilde{h_i} = h_i + (K(\pi/b)^2 + \gamma\lambda)p_i$. Using this approximation (therefore $\partial_x P = \frac{\mathrm{d}P}{\mathrm{d}x}$), the symmetry $v_x(x,0) = v_x(x,b)$ and the viscous friction $\sigma_{zx}(z=0) = \xi v_x(x,0)$, as in Section 2.2., this is solved by:

$$v_x(x,z) = -\frac{1}{2\eta}\frac{\mathrm{d}P}{\mathrm{d}x}\left((b-z)z + \frac{b\eta}{\xi}\right) - \frac{b\tilde{\zeta}\Delta\mu}{4\pi\eta}(1+\cos 2\theta) \tag{3.5}$$

and with the incompressibility condition equation (2.2)

$$v_z(x,z) = \frac{1}{12\eta}\frac{\mathrm{d}^2P}{\mathrm{d}x^2}\left((3b-2z)z + \frac{6b\eta}{\xi}\right)z - \frac{\mathrm{d}P}{\mathrm{d}x}\frac{\mathrm{d}\xi}{\mathrm{d}x}\frac{bz}{2\xi^2} + v_z(x,0) + \frac{b}{4\pi\eta}\frac{\mathrm{d}\tilde{\zeta}\Delta\mu}{\mathrm{d}x}\left(z + \frac{b\sin 2\theta}{2\pi}\right). \tag{3.6}$$

For polarisation with anchoring at each wall the same (e.g. parallel to the walls $\theta = 0$) there will be no flow. However a finite gradient in the polarisation, imposed for example by normal anchoring $\theta = -\frac{\pi}{2}(1 - \frac{2z}{b})$, gives a finite velocity as shown in Figure 8.

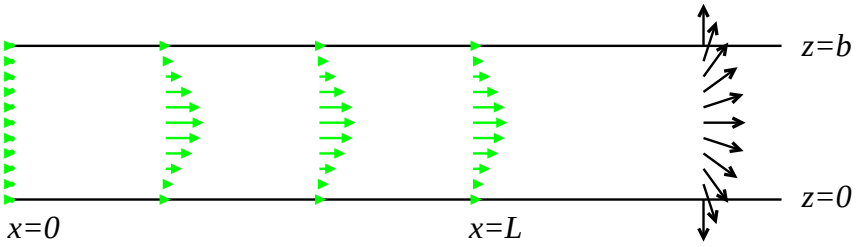


Figure 8: Polarisation $\theta = -\frac{\pi}{2}(1 - \frac{2z}{b})$ (black arrows) and velocity profile (equations (3.5) and (3.6)) (green, filled arrow heads) of an active gel in a channel.

The average velocity along the channel (equation 2.6) with the active contribution therefore becomes;

$$v(x) = -\frac{b^2}{12\eta}\left(1+\tilde{\xi}^{-1}\right)\frac{\mathrm{d}P}{\mathrm{d}x} - \frac{b\tilde{\zeta}\Delta\mu}{4\pi\eta},$$

which is a generalised Darcy's law.

## 3.4. Active gel with polymerisation at the walls

Introducing polymerisation at the walls as in Section 2.3. will affect the polarisation such that $\theta(z) = \theta_0 + \theta_1$ where $\theta_0 = -\frac{\pi}{2}(1-\frac{2z}{b})$ is the static configuration which satisfies the normal anchoring boundary condition as in Section 3.1. With the assumption that $\theta_1$ is linear in $v_p^0$, in the lubrication approximation (as outlined in Section 3.3.) to lowest order the polarisation is given by its static configuration $\theta_0$. Therefore the velocity is given by equations (3.5) and (3.6) with the de-polymerisation term $-k_d z$ in equation (3.6) as explained in Section 2.3. Experimental observations [18] indicate that the concentration of myosin is greater at the back of the cell. We model this with a simple linear gradient in the activity coefficient

$$\tilde{\zeta}(x)\Delta\mu = \tilde{\zeta}_0\Delta\mu(L-x)/L$$

The resulting velocity profile is shown in dashed green arrows in Figure 9, and shows that the contractile activity of the acto-myosin system enhances motion.

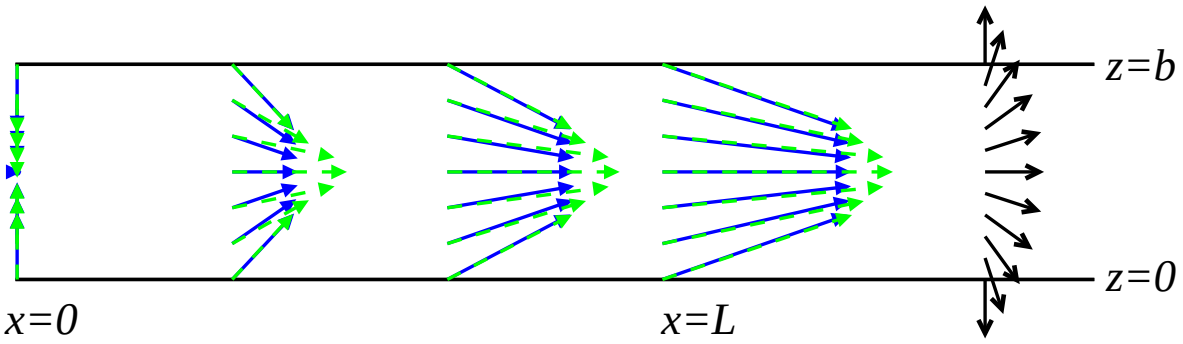


Figure 9: Polarisation (black) and flow velocity (equations (2.4) and (2.5)) with (dashed green) and without (blue) myosin. Polarisation arrows point in the direction of actin polymerisation. The active term is taken as $\tilde{\zeta}(x)\Delta\mu = \tilde{\zeta}_0\Delta\mu(L-x)/L$ for $x > 0$ such that there are more myosins at the back of the cell.

# 4. Tilted channel walls

In order to further investigate the role of geometric confinement on motility we consider a channel with one wall tilted such that the channel has the shape of a funnel (as shown in Figure 10). In this section we first consider a self-polymerising gel in such a channel, then an active contractile gel and finally adding both effects together.

## 4.1. Polymerising gel in tilted channel

In this geometry of a funnel shaped channel with the top wall tilted, the height of the channel is $b = b_0 + b_1 x$ (see Figure 10). Throughout we consider a small tilt $b_1 L \ll b_0$ keeping up to linear order in $b_1$. We substitute this into equations (2.4) and (2.5), calculating the pressure as outlined above in Section 2.7. The boundary conditions for the velocity perpendicular to the channel walls due to polymerisation become $v_\perp(x,0) = v_z(x,0) = v_p$ (as before) and $v_\perp(x,b) = v_z(x,b)\cos b_1 - v_x(x,b)\sin b_1 = -v_p$ (modified according to the new geometry). The velocity parallel to the channel walls becomes $v_x(x,0) = v_x(x,0)$ (as before) and $v_\parallel(x,b) = v_x(x,b)\cos b_1 + v_z(x,b)\sin b_1$ modified due to the tilted upper wall. Therefore the velocity components at the upper wall are now $v_x(x,b) = v_x(x,0)\cos b_1 + v_p \sin b_1$ and $v_z(x,b) = -v_p \cos b_1 + v_x(x,0)\sin b_1$. As before $v_x(x,0)$ is determined by the viscous friction $\sigma_{zx}(z=0) = \xi v_x(x,0)$ but the friction condition at the upper wall becomes $\sigma_\parallel(z=b) = \xi v_\parallel(x,b)$.

Intuitively we expect the material to flow towards the wider part of the channel since the polymerisation pushes off the tilted wall. However due to the conservation of mass (equation (2.7)) the average velocity $v$ in the tilted case will be slower than the straight case as the width $b$ becomes larger. The velocity profile in a straight (solid blue, filled arrow heads) compared to tilted (dashed red, filled arrow heads) channel is shown in Figure 10, assuming the pressure remains high enough for forward motion.

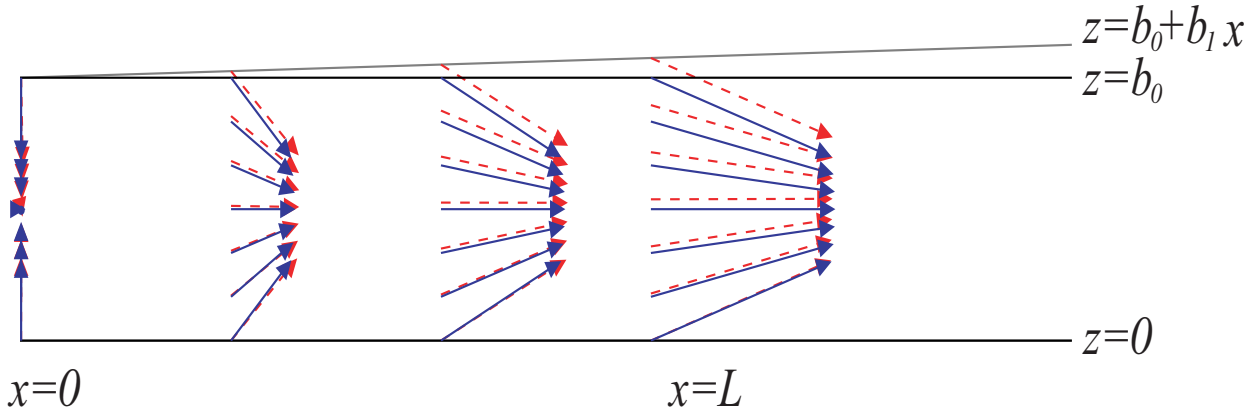


Figure 10: Velocity profile of a passive polymerising gel in a straight (solid blue, filled arrow heads) and tilted (dashed red, filled arrow heads) channel.

At this point it is appropriate to comment on the direction of movement. For a straight channel the symmetry is broken spontaneously and the cell is just as likely to move in the positive or negative $x$ direction. In the above we always chose the positive $x$ direction. For a tilted channel the tilt induces a preference for movement towards the wider part of the channel due to the polymerisation against the tilted wall. With motion towards the wider part, the pressure build-up towards the back increases faster than if the symmetry was broken in the opposite direction, due to the tilted geometry favouring a higher pressure in the narrower region. If the back was at the wider part, in an extreme case the pressure would not reach the threshold $P^*$ required for the mechanism we describe. These two effects of the polymerisation direction and the pressure give a bias to the symmetry breaking in favour of the positive $x$ direction.

## 4.2. Active contractile gel in tilted channel

In this section we ignore the possibility of self-polymerisation and consider an active contractile gel in a tilted channel. In this case the velocity is given by the equations (3.5) and (3.6) where $b = b_0 + b_1 x$ and the polymerisation velocity and depolymerisation rate are zero $v_p = k_d = 0$. Therefore the boundary conditions for the velocity components are $v_x(x, 0) = v_x(x, 0)$, $v_x(x, b) = v_x(x, 0) \cos b_1$, $v_z(x, 0) = 0$ and $v_z(x, b) = v_x(x, 0) \sin b_1$. The polarisation is taken with normal anchoring at the channel walls such that $\theta = -\frac{\pi}{2}(1 - \frac{2z}{b}) + \frac{b_1 z}{b}$. Figure 11 shows the polarisation and velocity profile for straight and tilted channels.

It is interesting to note that, for a long system the symmetry breaking would actually be biased in the direction as drawn in Figure 11(c) and not Figure 11(b) in order to minimise the elastic energy (equation 3.2). In this case the velocity is towards the narrower part of the channel. In the case of a finite cell within the channel with the polarisation normally outwards around the entire membrane surface, there is by necessity a defect. Minimising the elastic energy would favour the defect in the wider part of the channel and therefore the case drawn in Figure 11(c) where the direction of motion is towards the narrower part of the channel. This suggests that the symmetry breaking bias is in opposite directions for motion driven by polymerisation and motion driven by active contractility by molecular motors.

## 4.3. Active contractile and polymerising gel in tilted channel

Finally we consider a polymerising active gel in a tilted channel. We assume that the polymerisation is the dominant effect and therefore the symmetry breaking for the polarisation is in the positive $x$ direction towards the wider part of the channel as discussed in Section 4.1. The velocity profile is calculated from equations (3.5) and (3.6) with $b = b_0 + b_1 x$ and $\theta = -\frac{\pi}{2}(1 - \frac{2z}{b}) + \frac{b_1 z}{b}$. The boundary conditions for the velocity induced by the polymerisation are the same as those given in Section 4.1. The result is plotted in Figure 12 as solid brown filled arrow heads with the passive result from Section 4.1. (Figure 10) shown in dashed red filled arrow heads for comparison. With

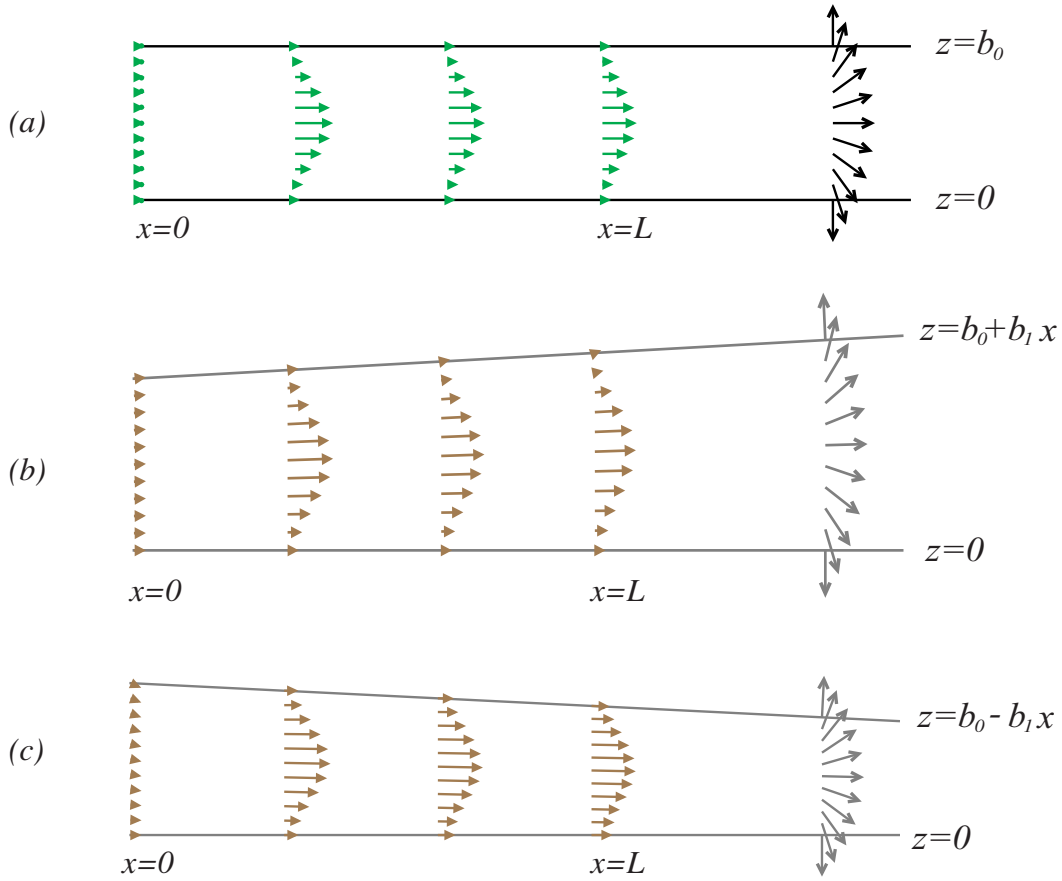


Figure 11: Velocity profile of an active gel in (a) straight (green filled arrow heads: velocity; black arrows: polarisation) and (b) tilted up (c) tilted down (brown filled arrow heads: velocity; grey arrows: polarisation) channel.

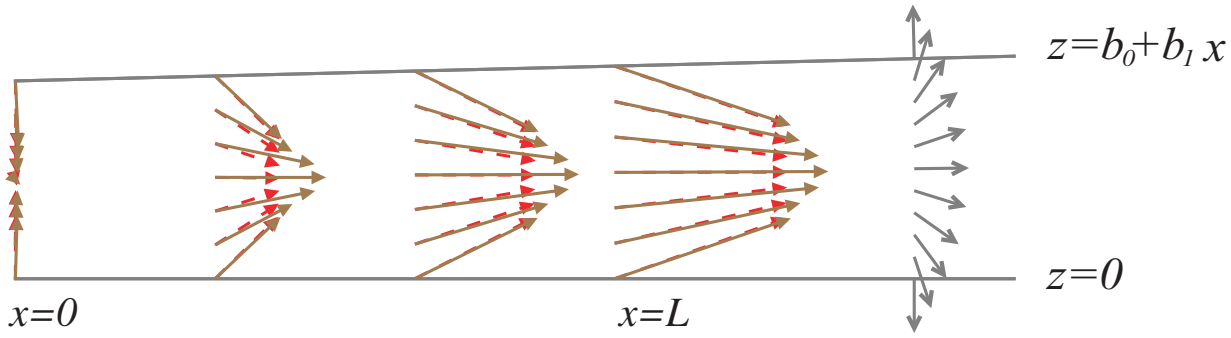


Figure 12: Velocity profile of a passive (dashed red, filled arrow heads) and active (solid brown, filled arrowheads) polymerising gel in a tilted channel, polarisation grey arrows

this choice of symmetry breaking it is clear that the effects of polymerisation, active contractility and a positive tilt in the confining walls are additive increasing the velocity in the channel in the positive $x$ direction (towards the wider part of the channel).

# 5. Conclusions

In conclusion, we have discussed mechanisms for cell motility in confinement which differ substantially from the standard picture of cell motility on flat open surfaces. Importantly our model does not require specific adhesion proteins since the mechanism relies on a pressure build-up in confinement which enhances the friction. This result is compatible with the experiments of [18], where it is found that integrin knocked out dendritic cells are motile only in confined environments. Within our model, which relies on actin polymerisation against the confining walls, contractility due to myosin molecular motors is not essential to motion but we show it can increase the speed, in agreement with experiments [18]. Finally we have also discussed motility in channels with tilted walls. We show that polymerisation against the confining walls alone is sufficient for cell motion in confinement. Also active contractility alone can produce motion if the local polarisation of the gel is anchored in such a way as to maintain a gradient of polarisation. We find that a combination of both effects can be additive, increasing the flow velocity.

# Acknowledgements

We thank Jean-François Joanny, Jacques Prost, Matthieu Piel, Olivier Collin and Ana-Maria Lennon-Duménil for helpful discussions.

# References

[1] B. Alberts. Molecular biology of the cell, 4th ed., Garland Science, New York, 2002.

[2] A. Bernheim-Groswasser, S. Wiesner, R. M. Golsteyn, M. F. Carlier, C. Sykes. *The dynamics of actin-based motility depend on surface parameters*, Nature, 417 (2002), No. 6886, 308–311.

[3] A. C. Callan-Jones, J.-F. Joanny, J. Prost. *Viscous-fingering-like instability of cell fragments*, Phys. Rev. Lett., 100 (2008), 258106.

[4] Y. Calle, S. Burns, A. J. Thrasher, G. E. Jones. *The leukocyte podosome.*, Eur. J. Cell. Biol., 85 (2006), No. 3-4, 151–157.

[5] C. Le Clainche, M.-F. Carlier. *Regulation of actin assembly associated with protrusion and adhesion in cell migration.*, Physiol. Rev., 88, (2008), No. 2, 489–513.

[6] M. Dogterom, M.E. Janson, C. Faivre-Moskalenko, A. van der Horst, J.W.J. Kerssemakers, C. Tanase, B.M. Mulder. *Force generation by polymerizing microtubules*, Applied Physics A: Materials Science & Processing, 75 (2002), No. 2, 331–336.

[7] C. Dombrowski, L. Cisneros, S. Chatkaew, R. E. Goldstein, John O. Kessler. *Self-concentration and large-scale coherence in bacterial dynamics*, Phys. Rev. Lett., 93 (2004), No. 9, 098103.

[8] G. Faure-André, P. Vargas, M.-I. Yuseff, M. Heuzé, J. Diaz, D. Lankar, V. Steri, J. Manry, S. Hugues, F. Vascotto, J. Boulanger, G. Raposo, M.-R. Bono, M. Rosemblatt, M. Piel, A.-M. Lennon-Duménil. *Regulation of dendritic cell migration by CD74, the MHC class II-associated invariant chain.*, Science, 322 (2008), No. 5908, 1705–1710.

[9] F. Gerbal, P. Chaikin, Y. Rabin, J. Prost. *An elastic analysis of listeria monocytogenes propulsion.*, Biophys. J., 79 (2000), No. 5, 2259–2275.

[10] P. G. de Gennes, J. Prost. The Physics of Liquid Crystals. Oxford. Univ. Press, Oxford, 1993.

[11] Y. Hatwalne, S. Ramaswamy, M. Rao, R. A. Simha. *Rheology of active-particle suspensions.*, Phys. Rev. Lett., 92 (2004), No. 11, 118101.

[12] R. J. Hawkins, M. Piel, G. Faure-Andre, A. M. Lennon-Dumenil, J. F. Joanny, J. Prost, R. Voituriez. *Pushing off the walls: a mechanism of cell motility in confinement.*, Phys. Rev. Lett., 102 (2009), No. 5, 058103.

[13] S. F. G. van Helden, D. J. E. B. Krooshoop, K. C. M. Broers, R. A. P. Raymakers, C. G. Figdor, F. N. van Leeuwen. *A critical role for prostaglandin e2 in podosome dissolution and induction of high-speed migration during dendritic cell maturation.*, J. Immunol., 177 (2006), No. 3, 1567–1574.

[14] F. Julicher, K. Kruse, J. Prost, J. F. Joanny. *Active behavior of the cytoskeleton*, Physics Reports, 449 (2007), No. 1-3, 3–28.

[15] K. Kruse, J. F. Joanny, F. Jülicher, J. Prost, K. Sekimoto. *Asters, vortices, and rotating spirals in active gels of polar filaments.*, Phys. Rev. Lett., 92 (2004), No. 7, 078101.

[16] K. Kruse, J. F. Joanny, F. Jülicher, J. Prost, K. Sekimoto. *Generic theory of active polar gels: a paradigm for cytoskeletal dynamics.*, Eur. Phys. J. E Soft Matter, 16 (2005), No. 1, 5–16.

[17] K. Kruse, J. F. Joanny, F. Jülicher, J. Prost. *Contractility and retrograde flow in lamellipodium motion.*, Phys Biol, 3 (2006), No. 2, 130–137.

[18] T. Lämmermann, B. L. Bader, S. J. Monkley, T. Worbs, R. Wedlich-Söldner, K. Hirsch, M. Keller, R. Förster, D. R. Critchley, R. Fässler, M. Sixt. *Rapid leukocyte migration by integrin-independent flowing and squeezing.*, Nature, 453 (2008), No. 7191, 51–55.

[19] R. Larson. Constitutive equations for polymer melts and solutions. Butterworth-Heinemann, 1998.

[20] T. B. Liverpool, M. C. Marchetti. *Instabilities of isotropic solutions of active polar filaments.*, Phys Rev Lett, 90 (2003), No. 13, 138102.

[21] S. E. Malawista, A. de Boisfleury Chevance. *Random locomotion and chemotaxis of human blood polymorphonuclear leukocytes (pmn) in the presence of edta: Pmn in close quarters require neither leukocyte integrins nor external divalent cations.*, Proc. Natl. Acad. Sci. USA, 94 (1997), No. 21, 11577–11582.

[22] D. Marenduzzo, E. Orlandini, M. E. Cates, J. M. Yeomans. *Steady-state hydrodynamic instabilities of active liquid crystals: Hybrid lattice boltzmann simulations*, Phys. Rev. E, 76 (2007), No. 3, 031921 (English).

[23] D. Marenduzzo, E. Orlandini, M. E. Cates, J. M. Yeomans. *Lattice boltzmann simulations of spontaneous flow in active liquid crystals: The role of boundary conditions*, J. Non-Newton. Fluid Mech., 149 (2008), no. 1-3, 56–62.

[24] A. Mogilner, G. Oster. *Cell motility driven by actin polymerization*, Biophys J., 71 (1996), no. 6, 3030–3045.

[25] V. Narayan, S. Ramaswamy, N. Menon. *Long-lived giant number fluctuations in a swarming granular nematic*, Science, 317 (2007), No. 5834, 105–108.

[26] F. J. Nedelec, T. Surrey, A. C. Maggs, S. Leibler. *Self-organization of microtubules and motors*, Nature, 389 (1997), No. 6648, 305–308.

[27] T. D. Pollard, G. G. Borisy. *Cellular motility driven by assembly and disassembly of actin filaments.*, Cell, 112 (2003), No. 4, 453–465.

[28] J. M. Serrador, M. Nieto, F. Sánchez-Madrid. *Cytoskeletal rearrangement during migration and activation of t lymphocytes.*, Trends. Cell. Biol., 9 (1999), No. 6, 228–233.

[29] R. A. Simha, S. Ramaswamy. *Hydrodynamic fluctuations and instabilities in ordered suspensions of self-propelled particles.*, Phys Rev Lett, 89 (2002), No. 5, 058101.

[30] J. A. Theriot, T. J. Mitchison. *Actin microfilament dynamics in locomoting cells.*, Nature, 352 (1991), No. 6331, 126–131.

[31] J. Toner, Y. Tu, S. Ramaswamy. *Hydrodynamics and phases of flocks.*, Annals of Physics, 318 (2005), No. 1, 170–244.

[32] R. Voituriez, J. F. Joanny, J. Prost. *Spontaneous flow transition in active polar gels*, Europhys. Lett., 70 (2005), No. 3, 404–410.

[33] R. Voituriez, J. F. Joanny, J. Prost. *Generic phase diagram of active polar films.*, Phys. Rev. Lett., 96 (2006), No. 2, 028102.

[34] P. T. Yam, C. A. Wilson, L. Ji, B. Hebert, E. L. Barnhart, N. A. Dye, P. W. Wiseman, G. Danuser, J. A. Theriot. *Actin myosin network reorganization breaks symmetry at the cell rear to spontaneously initiate polarized cell motility*, The Journal of Cell Biology, 178 (2007), No. 7, 1207–1221.

[35] A. Zumdieck, R. Voituriez, J. Prost, J. F. Joanny. *Spontaneous flow of active polar gels in undulated channels*, Faraday Discuss., 139 (2008), 369.